Switched-Capacitor Tuning for Three-Phase Wireless Power Receiver Based on Perturbation and Observation Method

CHAO WANG[ID]**[1], CHUNBO ZHU[1], (Member, IEEE), GUO WEI**[ID]**[1], JINGYANG ZHANG[1], AND FEI LIU[2]**

[1]Harbin Institute of Technology, Harbin 150001, China
[2]China Academy of Launch Vehicle Technology, Beijing 100076, China

Corresponding author: Guo Wei (hitweiguo@hit.edu.cn)

ABSTRACT To realize the tuning of three-phase dynamic wireless power receivers for rail vehicles, a non-real-time static self-tuning scheme based on the switched capacitor and the perturbation and observation (P&O) method is studied. First, the reactance regulation characteristics of the parallel and the series switched capacitor are discussed and compared. Then, to avoid the sophisticated mistuning detection, in the case of only observing the output voltage, the feasibility of using the P&O method to tune three phases of the receiver sequentially is analyzed. Furthermore, theoretical analysis shows that the switched capacitor can also be used to control the current phase difference between the three phases. Thereby, by introducing the current phase difference control, a fast three-phase simultaneous tuning strategy is proposed without additional hardware. Afterward, the self-tuning control scheme for the star-connected series-compensated receiver with the parallel and series switched capacitor is design in detail and be applied to a scaled-down prototype of a three-phase dynamic wireless power transfer system for verification. The result shows that the receiver can be tuned within the ±5% deviation of the main compensation capacitance, and the tuning speed of the proposed simultaneous tuning of three phases is about three times that of the sequence tuning.

INDEX TERMS Perturbation and observation (P&O), switched capacitor, self-tuning, three-phase, wireless power transfer (WPT).

I. INTRODUCTION

Wireless power transfer (WPT) can transmit electricity through magnetic field coupling, which has the advantages of convenience, safety, and beauty [1]. In the field of electric vehicle application, WPT technology provides convenience for charging. However, the charging of the battery still takes a long time. In order to eliminate the time occupation of charging, dynamic WPT (DWPT) has been proposed [2]–[4]. DWPT refers to powering the vehicle during driving, which avoids parking to recharge [2]–[4]. Compared with the traditional contact power supply, DWPT has various advantages such as all-weather adaptation, no electrocution hazard during accidents, lower maintenance, and beauty in the field of rail transit. Among the existing DWPT systems, the three-phase meander-type DWPT system shown in FIGURE 1

The associate editor coordinating the review of this manuscript and approving it for publication was Poki Chen[ID].

is characterized by the low lateral magnetic field exposure and high power transmission capability [8], [9]. Although compared with the single-phase system, the structure of the three-phase system is more complex, which leads to lower reliability and higher cost, and the interaction and balance of the three phases need to be considered in the design. The three-phase meander-type DWPT system still shows high practical in rail transit due to the steel rail and high power demand.

Because of the fast speed of the vehicle, the working frequency and currents of the transmitting coils in the DWPT system are usually fixed to stabilize the power transmission [7], [10]. Thus, in the stable coupling, the power receiver with the series compensation topology can output the constant voltage to meet the requirement of general power systems. However, in practical applications, due to the influence of the manufacturing accuracy, installation environment, aging, and other factors, the reactive power compensation of transmitters
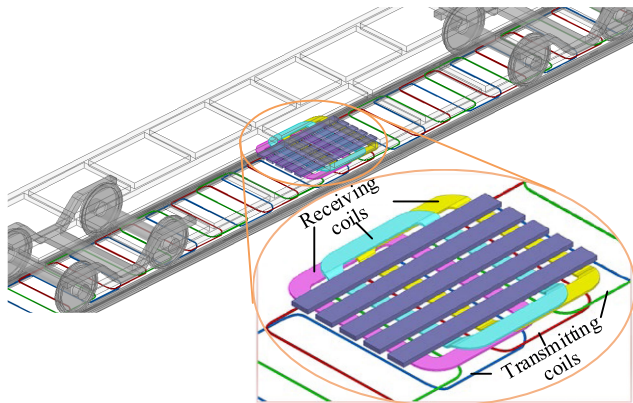
FIGURE 1. Coupler structure of the three-phase meander-type DWPT system for railway vehicle applications.

and receivers may significantly deviate from the ideal value, and thus mistuning is occurred [11], [12]. The resulting power transmission characteristics will deviate from the design expectations, and the active power transfer capacity and system efficiency will be reduced. Therefore, it is necessary to tune the WPT system to achieve efficient and stable power transmission.

In practice, different installation environments have different effects on the coil inductance. Thus the simple and straightforward tuning method is to measure the coil inductance and compensation capacitance on-site and then match them. However, this can lead to high labor costs, so it is not suitable for large volume applications. Besides, the parameters of coils and capacitors must be highly stable, which leads to high manufacturing costs. Otherwise, regular calibration is required, which further increases the labor cost. A better way is to tune the system by itself.

Self-tuning is usually realized by adjusting inductance or capacitance. In [13], inductance regulation is achieved by a magnetic amplifier. However, because the compensation circuit does not necessarily contain inductors but must have capacitors, and the adjustable inductor volume is large, the tuning method by regulating capacitance is more commonly used. The existing ways to realize capacitance regulating include the capacitor matrix [14]–[16], voltage-controlled capacitor [17], and switched capacitor [12], [18], [25]. In addition to the mentioned three methods, the controlled rectifier or an inductor paralleled with load can also be used for tuning at the receiver [11], [19].

The capacitor matrix has the advantages of simple and reliable control and can realize tuning by selecting appropriate capacitors. But this requires many switches and capacitors, and the method cannot continuously adjust reactance [15]. The voltage-controlled capacitor can realize continuous tuning, but it is only suitable for the case of small power [17]. The switched capacitor is investigated to overcome the issues, which can realize continuous tuning and can be implemented in high-power applications [12], [18]. However, the existing studies mainly focus on transmitter tuning and lack in-depth

consideration of the receiver tuning. In the current receiver tuning research, the full-bridge controlled rectifier is used for single-phase receiver tuning, but it is too complex to be used for a three-phase receiver [12], [18]. The tuning method utilizing an inductor paralleled with load significantly increases the system volume and structure complexity [11].

Compared with the transmitter, the phase of the induced voltage at the receiver cannot be measured directly, so it is difficult to judge the degree of mistuning. [11] and [19] proposed adding a detection coil to detect the phase of the induced voltage. But there is a coupling between the detection coil and the receiving coil. The accurate phase-detection requires good decoupling, which is difficult to achieve in large volume applications. Furthermore, in three-phase systems, the phase-detection of induced voltages is more complicated than that in single-phase systems due to the mutual interference between three phases. However, there is little research on the self-tuning of the three-phase systems at present.

For the three-phase receiver, the mistuning reduces the system efficiency and causes the three-phase imbalance. To obtain the accurate degree of mistuning in the three-phase receiver, the phases of the positive sequence voltage and the positive sequence current are required to detect simultaneously. However, because of the mutual coupling between the three phases, the positive sequence component of the induced voltage is challenging to detect. Besides, the detection of the positive sequence current further increases the complexity of mistuning detection. Therefore, a practical and straightforward tuning method for the three-phase system is expected.

In fact, the influence of the manufacturing process and installation environment on the mistuning is constant, and the change of parameters caused by the temperature, aging, and other factors is slow. Thus, the demand for real-time tuning is not urgent. As a compromise, the DWPT system can be tuned when the vehicle stops at stations. On the other hand, the output voltage under the resonance state is the maximum when the receiver's induction voltage and load are constant. Therefore, while keeping the transmitter working state, coupling relationship, and load state unchanged, the perturbation and observation (P&O) method (also called the hill-climbing method) can be used to determine whether the resonance has been achieved by observing the output voltage of receivers [20], [21]. The concept of tuning the three-phase system by the P&O method also can be found in [21]. However, only simulation analysis is performed in the paper, and physical experiment verification and analysis of actual application characteristics (such as adjustment effect and speed) are lacking.

To realize the tuning of the three-phase receiver, the switched-capacitor tuning with the P&O method is studied in this paper. In section II, the reactance regulation characteristics of the parallel and series switched capacitor are analyzed and compared. In section III, the receiver tuning characteristics of the P&O method based on output voltage observation are analyzed to verify the feasibility. Furthermore, Theoretical analysis shows that the switched capacitor can

also be used to control the current phase difference between three phases, and the mistuning degrees of three phases are identical when the phase differences between the currents of three phases equal that of the induced voltages of three phases. Thereby, by introducing the additional current phase difference control, a fast simultaneous tuning strategy of three phases is proposed without additional hardware. In section IV, the self-tuning control scheme for the star-connected series-compensated receiver with the parallel and series switched capacitor is designed in detail. The experimental verification is conducted in section V. Finally, the conclusion is summarised in section VI.

II. REACTANCE REGULATION CHARACTERISTICS OF SWITCHED CAPACITORS

A. PARALLEL SWITCHED CAPACITOR

The common connection mode of the switched capacitor and the main capacitor is the parallel connection. For the switched capacitor, the switch type can be divided into bidirectional controllable and unidirectional controllable. Compared with the unidirectional controllable, the device stress of the bi-directional controllable switch is reduced by half. However, unidirectional control is easier to implement and verify, and thus only the unidirectional controllable switch is analyzed.
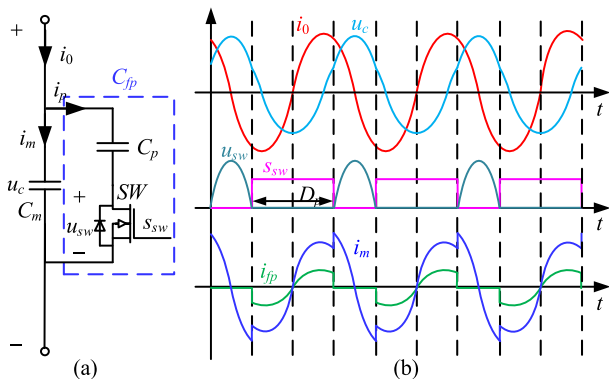

FIGURE 2. (a) Schematic of the parallel switched capacitor and (b) waveforms in the ideal switching process.

The schematic of the parallel switched capacitor and the waveforms of the ideal switching process are shown in FIGURE 2, in which C_m is the main compensation capacitance, C_p is the parallel capacitance, SW is the controlled switch, i_0 is the total current, i_m is the current of C_m, i_p is the current of C_p, u_{sw} is the voltage of SW, s_{sw} is the control signal of SW, D_p is the duty cycle of s_{sw}, and C_{fp} is the equivalent parallel capacitance. As shown in FIGURE 2 (b), SW can be turned on at zero voltage and turned off with a low dv/dt rate. Thus the switching loss is small, which is highly practical.

In WPT systems, the compensation circuit topology is characterized by band-pass filtering, so the harmonic components of i_0 can be ignored. The current i_0 can be expressed

as

$$i_0 = \sqrt{2}I_0 \sin(\omega_0 t) \tag{1}$$

where I_0 is the RMS of the fundamental component of i_0, and ω_0 is the working angular frequency. Then, i_m can be expressed as

$$i_m = \begin{cases} i_0 C_m/(C_m + C_p) & SW \text{ on} \\ i_0 & SW \text{ off} \end{cases} \tag{2}$$

According to Fourier expansion, the RMS of the fundamental component of i_m can be derived as

$$I_m = \frac{2}{\pi} \int_0^\pi i_m \sin(\omega_0 t) \, \mathrm{d}\omega_0 t$$
$$= I_0 \left\{ 1 - \left[D_p - \sin(2\pi D_p)/4 \right] C_p/(C_m + C_p) \right\} \tag{3}$$

Then, C_{fp} can be calculated according to the equal voltage relationship and is written as

$$\omega_0 C_{fp} I_m = \omega_0 C_m (I_0 - I_m)$$
$$\Rightarrow C_{fp} = C_m (I_0/I_m - 1) \tag{4}$$

Defining g_p as the capacitive reactance gain of the parallel switched capacitor, we get

$$g_p = \frac{1/\left[j\omega_0 (C_m + C_{fp}) \right]}{1/(j\omega_0 C_m)} = \frac{I_m}{I_0}$$
$$= 1 - \alpha \left[D_p - \sin(2\pi D_p)/4 \right] \tag{5}$$

where $\alpha = C_p/(C_m + C_p)$. FIGURE 3 shows the relationship between g_p, α, and D_p. As can be seen from the figure, the parallel switched capacitor can continuously reduce the capacitive reactance of the compensation capacitors by increasing D_p. When $D_p = 1$, the minimum g_p can be obtained, and the value is $1 - \alpha$.
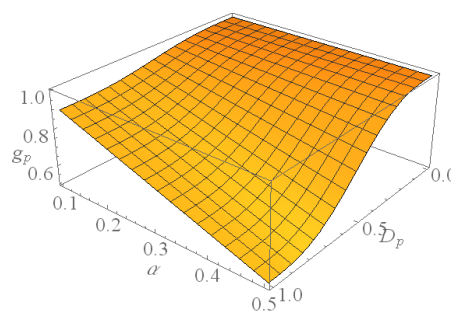

FIGURE 3. g_p vs. α and D_p.

B. SERIES SWITCHED CAPACITOR

In previous literature, most switched capacitors and the main compensation capacitors are connected in parallel. The parallel switched capacitors require the same voltage rating as the main compensation capacitors, which makes the selection of capacitors more convenient. However, the series switched capacitor has a similar capacitive reactance regulation capability and requires a lower device voltage rating [25]. Therefore, it can also be used as an alternative or supplement,

especially for high voltage applications. The schematic of the series switched capacitor is shown in FIGURE 4, where C_s is the series capacitance, i_s is the current of C_s, and C_{fs} is the equivalent capacitance of the series switched capacitor. As shown in FIGURE 4 (b), similarly to the parallel situation, SW can also be turned on at zero voltage and turned off with a low dv/dt rate. Thus the switching loss is small too.
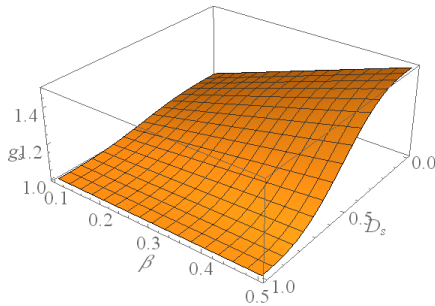

FIGURE 4. g_s vs. β and D_s.

Similarly to the parallel situation, i_s can be expressed as

$$i_s = \begin{cases} 0 & SW \ \text{on} \\ i_0 & SW \ \text{off} \end{cases} \tag{6}$$

According to Fourier expansion, the RMS of the fundamental component of i_s can be derived as

$$I_s = \frac{2}{\pi} \int_0^\pi i_s \sin(\omega_0 t) \, d\omega_0 t$$
$$= I_0 \{1 - D_s - \sin[2\pi(1 - D_s)]/4\} \tag{7}$$

Then, C_{fs} can be calculated according to the equal voltage relationship and is written as

$$\omega_0 C_{fs} I_s = \omega_0 C_s I_0 \Rightarrow C_{fs} = C_s I_0 / I_s \tag{8}$$

Defining g_s as the capacitive reactance gain of the series switched capacitor, we get

$$g_s = \left(\frac{1}{j\omega_0 C_m} + \frac{1}{j\omega_0 C_{fs}} \right) \bigg/ \frac{1}{j\omega_0 C_m}$$
$$= 1 + \beta \{1 - D_s - \sin[2\pi(1 - D_s)]/4\} \tag{9}$$

where $\beta = C_m/C_s$. The relation between g_s, β, and D_s. is shown in FIGURE 5. Contrary to the parallel situation, the series switched capacitor can continuously increase the capacitive reactance of the compensation capacitors by increasing D_s. When $D_s = 1$, g_s is maximum, and the value is $1 + \beta$.

C. COMPARISON OF PARALLEL AND SERIES SWITCHED CAPACITORS
The characteristic comparison between parallel and series switched capacitor circuits can be obtained based on the above analysis, as shown in TABLE 1. Although one of the capacitive reactance gain regulation ranges of the two
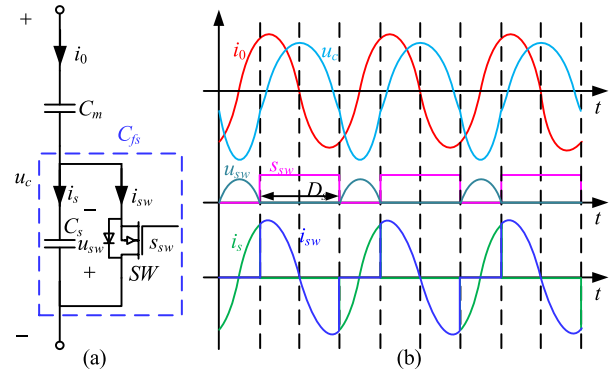

**FIGURE 5.** (a) Schematic of series switched capacitor and (b) waveforms in the ideal switching process.

TABLE 1. Characteristic comparison of parallel and series switched capacitor circuits.

Circuit structure	Capacitive reactance gain regulation range	Max. voltage stress of switch	Max. current stress of switch	Max. voltage stress of switched capacitor
Parallel switched capacitor	$1 - \dfrac{C_p}{C_m + C_p} \sim 1$	$\dfrac{2\sqrt{2}I_0}{\omega C_m}$	$\dfrac{\sqrt{2}IC_p}{{}^0 C_m + C_p}$	$\dfrac{\sqrt{2}I_0}{\omega C_m}$
Series switched capacitor	$1 \sim 1 + \dfrac{C_m}{C_s}$	$\dfrac{2\sqrt{2}I_0}{\omega C_s}$	$\sqrt{2}I_0$	$\dfrac{2\sqrt{2}I_0}{\omega C_s}$

circuits is always greater than 1 and the other is always less than 1, bidirectional adjustment of capacitive reactance can be realized by biasing the main compensation capacitance. On the other hand, compared with using only parallel or series switched capacitors, the parallel and series switched capacitors can be used in combination to reduce the device rating within the same regulation range or obtain a wider regulation range under the same device rating. Also, it can be seen that the maximum voltage and current stress of the switch in the parallel switched capacitor circuit are C_s/C_m and $C_p/(C_m + C_p)$ times those of the switch in the series capacitor circuit, respectively. The maximum voltage stress of the switched capacitor in the parallel circuit is $C_s/(2C_m)$ times that of the switched capacitor in the series circuit.

III. RECEIVER TUNING CHARACTERISTICS OF P&O METHOD BASED ON OUTPUT VOLTAGE OBSERVATION
In the WPT system, to tune the receiver, besides the specific means of reactance adjustment, the direction of regulation needs to be known. The most direct method is to measure the phase difference between induced voltage and current. However, this requires an additional induced voltage phase-detection coil, which increases the complexity of the system. Moreover, for the three-phase system, the positive sequence components of voltage and current are needed to be further calculated. Besides, the actual detection accuracy is difficult to guarantee. Since the output of the receiver will be affected by mistuning, it is possible to use the P&O method to search for the maximum output voltage to realize the tuning of the receiver.
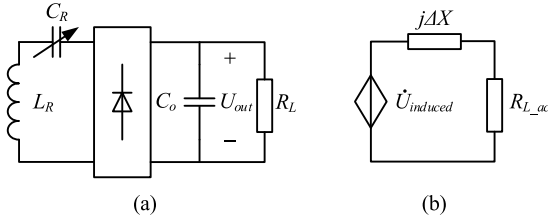
**FIGURE 6.** (a) Schematic of series compensated single-phase receiver and (b) AC equivalent circuit.

A. SINGLE-PHASE RECEIVER

The schematic of a series compensated single-phase receiver is shown in FIGURE 6(a), in which L_R is the inductance of the receiving coil, C_R is the adjustable compensation capacitance, C_o is the DC filter capacitance, R_L is the load resistance, U_{out} is the DC output voltage, and I_{out} is the DC output current. FIGURE 6(b) shows the AC equivalent circuit, where $\dot{U}_{induced}$ is the induction voltage, $j\Delta X$ is the uncompensated reactance, and R_{L_ac} is the load equivalent AC resistance. In the ideal case,

$$R_{L\_ac} = \frac{8}{\pi^2} R_L \qquad (10)$$

$$U_{out} = \frac{\pi^2}{8} \left| \frac{1}{1 + j\Delta X / R_{L\_ac}} \dot{U}_{induced} \right| \qquad (11)$$

Therefore, when $\left| \dot{U}_{induced} \right|$ and R_L is constant, U_{out} is the function of ΔX.
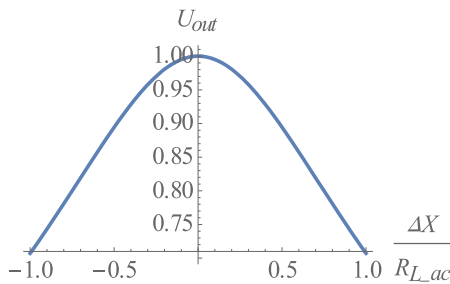
FIGURE 7. Relationship between normalized U_{out} and ΔX.

The relationship between U_{out} and ΔX after normalization is shown in FIGURE 7. It is evident that the receiver can be tuned by searching for the maximum value of U_{out}. Furthermore, the change of U_{out} is more significant when R_L is smaller. Since the tuning process is the process of finding the maximum output voltage, and the magnitude of perturbation is determined by one step of reactance regulation. The tuning accuracy will deteriorate when external interference on output voltage is more significant than that of single-step capacitive reactance adjustment. Therefore, to improve the tuning accuracy, a large output current should be maintained to increase the influence of the reactance regulation on the output voltage, and external interference should be reduced. Due to the limitation of the rated output current (I_{out_rated}) of the actual system, R_L cannot be less than U_{out}/I_{out_rated}.

Thus, the best tuning effect can be obtained in the regulation process when I_{out} is equal to I_{out_rated}.
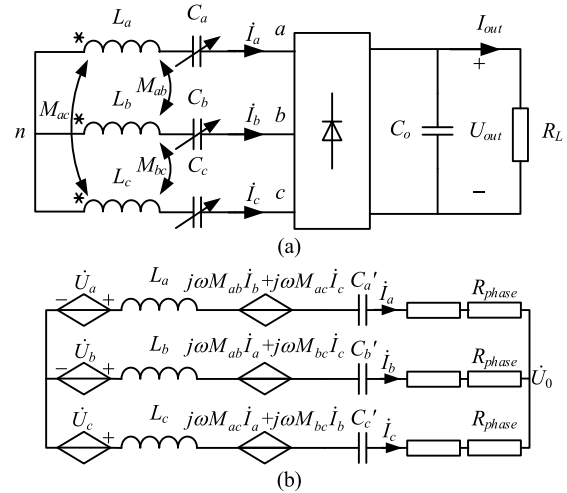
FIGURE 8. (a) Schematic of three-phase receiver with start-connection and series-compensation and (b) AC equivalent circuit.

B. THREE-PHASE RECEIVER

Compared with the single-phase receiver, the three-phase receiver is more complicated. For the tuning of the three-phase receiver, the effectiveness of P&O needs to be explored. FIGURE 8 shows the schematic of the three-phase receiver with star-connection and series-compensation and the AC equivalent circuit, wherein L_a, L_b, and L_c are the inductance of three receiving coils, C_a, C_b, and C_c are the adjustable compensation capacitance of three phases, $\dot{I}_a$, $\dot{I}_b$, and $\dot{I}_c$ are the current of three phases, n is the neutral point of three-phase induced voltage, $\dot{U}_a$, $\dot{U}_b$, and $\dot{U}_c$ are the induced voltage of three receiving coils, M_{ab}, M_{ac}, and M_{bc} are the mutual inductance between three receiving coils, C_a', C_b', and C_c' are the ideal compensation capacitance of three phases, $j\Delta X_a = j/(\omega_0 C_a) - j/(\omega_0 C_a')$, $j\Delta X_b = j/(\omega_0 C_b) - j/(\omega_0 C_b')$, and $j\Delta X_c = j/(\omega_0 C_c) - j/(\omega_0 C_c')$ are the uncompensated reactance of three phases, $R_{phase} = 6R_L/\pi^2$ is the equivalent AC load resistance of each phase, and $\dot{U}_0$ is the zero-sequence voltage caused by the difference of the self inductances and mutual inductances. C_a', C_b', and C_c' can be calculated as [22]

$$\begin{cases} C_a' = 1/[\omega_0^2(L_a - M_{ab} - M_{ac} + M_{bc})] \\ C_b' = 1/[\omega_0^2(L_b - M_{ab} - M_{bc} + M_{ac})] \\ C_c' = 1/[\omega_0^2(L_c - M_{ac} - M_{bc} + M_{ab})] \end{cases} \qquad (12)$$

According to Kirchhoff's Law,

$$\begin{cases} \dot{U}_a = R_{phase}\dot{I}_a + j\Delta X_a\dot{I}_a + j\omega_0 L_a\dot{I}_a + j\omega_0 M_{ab}\dot{I}_b \\ \quad + j\omega_0 M_{ac}\dot{I}_c + \dot{I}_a/(j\omega_0 C_a) + U_0 \\ \dot{U}_b = R_{phase}\dot{I}_b + j\Delta X_b\dot{I}_b + j\omega_0 L_b\dot{I}_b + j\omega_0 M_{ab}\dot{I}_a \\ \quad + j\omega_0 M_{bc}\dot{I}_c + \dot{I}_b/(j\omega_0 C_b) + U_0 \\ \dot{U}_c = R_{phase}\dot{I}_c + j\Delta X_c\dot{I}_c + j\omega_0 L_c\dot{I}_c + j\omega_0 M_{ac}\dot{I}_a \\ \quad + j\omega_0 M_{bc}\dot{I}_b + \dot{I}_c/(j\omega_0 C_c) + U_0 \\ \dot{I}_a + \dot{I}_b + \dot{I}_c = 0 \end{cases} \qquad (13)$$
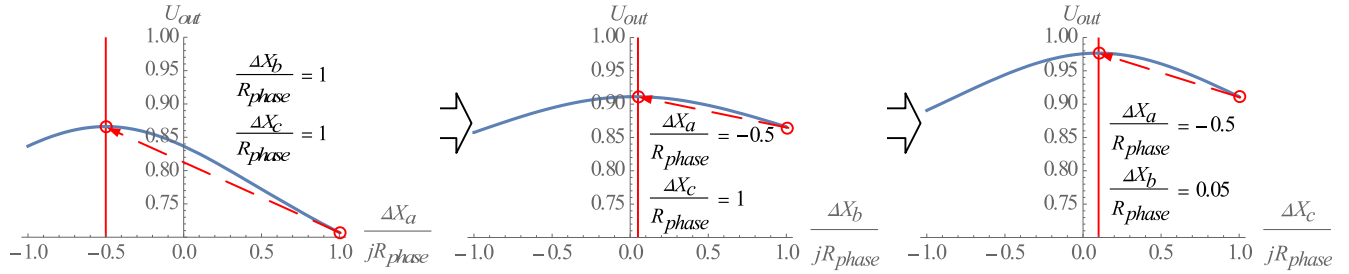
FIGURE 9. The normalized output voltage for phase a, b, and c are sequentially tuned by searching for the maximum output voltage.

Thereby, $\dot{I}_a$, $\dot{I}_b$, and $\dot{I}_c$ can be solved as

$$\begin{cases} \dot{I}_a = \left[\dot{U}_a \left(Z_b + Z_c \right) - \dot{U}_b Z_c - \dot{U}_c Z_b \right] / Z_m \\ \dot{I}_b = \left[\dot{U}_b \left(Z_a + Z_c \right) - \dot{U}_c Z_a - \dot{U}_a Z_c \right] / Z_m \\ \dot{I}_c = \left[\dot{U}_c \left(Z_a + Z_b \right) - \dot{U}_a Z_b - \dot{U}_b Z_a \right] / Z_m \end{cases} \quad (14)$$

where $Z_m = Z_a Z_b + Z_a Z_c + Z_b Z_c$, $Z_a = R_{phase} + j\Delta X_a$, $Z_b = R_{phase} + j\Delta X_b$, and $Z_c = R_{phase} + j\Delta X_c$. Furthermore, in the ideal case, assuming $\dot{U}_a = U_R \angle 0°$, then

$$\dot{U}_b = U_R \angle -120° \quad (15)$$
$$\dot{U}_c = U_R \angle 120° \quad (16)$$

On the other hand, U_{out} can be expressed as

$$U_{out} = \sqrt{\frac{P_a + P_b + P_c}{R_L}} = \sqrt{\frac{6 \left(P_a + P_b + P_c \right)}{\pi^2 R_{Phase}}} \quad (17)$$

where P_a, P_b, and P_c are the output power of each phase and are calculated as

$$\begin{cases} P_a = \text{Re}[\dot{U}_a]\text{Re}[\dot{I}_a] + \text{Im}[\dot{U}_a]\text{Im}[\dot{I}_a] \\ P_b = \text{Re}[\dot{U}_b]\text{Re}[\dot{I}_b] + \text{Im}[\dot{U}_b]\text{Im}[\dot{I}_b] \\ P_c = \text{Re}[\dot{U}_c]\text{Re}[\dot{I}_c] + \text{Im}[\dot{U}_c]\text{Im}[\dot{I}_c] \end{cases} \quad (18)$$

Therefore, when U_R and R_L are constant, the relationship between U_{out} and ΔX_a, ΔX_b, and ΔX_c can be obtained to further verify the feasibility of tuning by the P&O method.

1) TUNING THREE PHASES SEQUENTIALLY

The most intuitive way is to tune three phases sequentially. The effectiveness of tuning can be evaluated by analyzing the tuning characteristics in the case of maximum mistuning. Generally, the operational circuit quality factor is designed to be less than ten for practical operation conditions [1], and the error of coil inductances and compensation capacitances can be controlled within ±5% of the theoretical value. In this way, $\Delta X_a/R_{phase}$, $\Delta X_b/R_{phase}$, and $\Delta X_c/R_{phase}$ are in the range of −1 to 1 when the differences between the three phases are ignored. Thus, we can assume $\Delta X_a/R_{phase}$, $\Delta X_b/R_{phase}$, and $\Delta X_c/R_{phase} \in [-1, 1]$. Thus, for the maximum mistuning state, $\Delta X_a/R_{phase}$, $\Delta X_b/R_{phase}$, and $\Delta X_c/R_{phase}$ equal to 1 or −1. Only the case of $\Delta X_a/R_{phase} = \Delta X_b/R_{phase} = \Delta X_c/R_{phase} = 1$ is analyzed in this paper here due to the symmetry of the two cases.

FIGURE 9 shows the output voltage when phases a, b, and c are sequentially tuned by searching for the maximum output voltage. As shown in the figure, when $\Delta X_a/R_{phase} = \Delta X_b/R_{phase} = \Delta X_c/R_{phase} = 1$, U_{out} is the smallest, which is only 70.8% of the maximum value. After phase a, b, and c are tune, U_{out} is increased to 86.5%, 91.0%, and 97.8%, respectively. Although the receiver is not fully tuned after a round of adjustment, the adverse effect of mistuning on the output voltage has been significantly reduced.

In theory, the mistuning can be calibrated through multiple rounds of adjustment. However, long tuning time is consumed. In practice, there is always the uncompensated residual reactance in each phase due to the restriction of the measurement accuracy of the output voltage, external interference, and non-ideal devices. Moreover, the consistency of the residual reactance in three phases cannot be guaranteed, which is detrimental to the system's reliability.

2) TUNING THREE PHASES SIMULTANEOUSLY

When the three phases' impedance is the same, the phase differences of the current and induced voltage between the three phases are identical. Ideally, the induced voltage phase difference between any two phases equals 120°. Therefore, if the current phase difference between any two phases could be maintained at 120°, the three phases' impedance can be tuned at the same time. Since the phase detection can be carried out at high speed, this method can reduce the tuning time and keeps the three-phase current balance.

Additionally, the current phase detection function has been provided in the switched capacitor tuning circuit. Hence, it is easy to judge whether the three-phase balance is realized or not by detecting the phase difference.

According to (14), the current phase difference between phase a and b (θ_{ab}) satisfies

$$\frac{\dot{I}_a}{\dot{I}_b} = \left| \frac{\dot{I}_a}{\dot{I}_b} \right| e^{j\theta_{ab}} = \frac{Y_{n\_ab}}{Y_{d\_ab}} e^{j\frac{2\pi}{3}} \quad (19)$$

where $Y_{n\_ab} = 1 + j\Delta X_c/R_{phase} + (1 + j\Delta X_b/R_{phase})e^{-j\pi/3}$ and $Y_{d\_ab} = 1 + j\Delta X_a/R_{phase} + (1 + j\Delta X_c/R_{phase})e^{-j\pi/3}$. It can be seen that the phase angle of Y_{n_ab} monotonically increases with the increase of ΔX_b when $\left| \Delta X_b/R_{phase} \right| \leq \sqrt{3}$ and $\left| \Delta X_c/R_{phase} \right| \leq \sqrt{3}$, and the phase angle of Y_{d_ab} monotonically increases with the increase of ΔX_a when

$|\Delta X_b / R_{phase}| \leq \sqrt{3}$ and $|\Delta X_c / R_{phase}| \leq \sqrt{3}$. As mentioned above, $\Delta X_a / R_{phase}$, $\Delta X_b / R_{phase}$, and $\Delta X_c / R_{phase}$ are in the range of -1 to 1 for general systems. Therefore, θ_{ab} decreases monotonically with the increase of ΔX_a, and increases monotonically with the increase of ΔX_b.

In the same way, it can be proved that the current phase difference between phase b and c (θ_{bc}) decreases monotonically with the increase of ΔX_b, and increases monotonically with the increase of ΔX_c. Besides, the current phase difference between phase c and a (θ_{ca}) decreases monotonically with the increase of ΔX_c, and increases monotonically with the increase of ΔX_a.

Therefore, the current phase difference between the three phases can be maintained constant by increasing or decreasing $\Delta X_{a/b/c}$ and $\Delta X_{b/c/a}$ according to whether $\theta_{ab/bc/ca}$ and $\theta_{bc/ca/ac}$ are greater than the set values or not. Combining the P&O tuning method with the current phase difference control, the impedance of three phases can be tuned simultaneously, and the tuning performance is superior to that of tuning three phases sequentially.
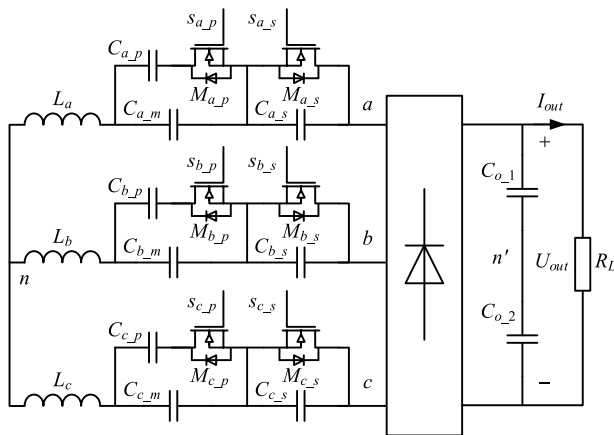
FIGURE 10. Circuit schematic of the star-connected series-compensated three-phase receiver with parallel and series switched capacitors.

IV. SYSTEM DESIGN

To verify the performance of the parallel and series switched capacitor tuning simultaneously, a circuit of a star-connected series-compensated three-phase receiver with parallel and series switched capacitors is designed as shown in FIGURE 10. In the figure, C_{a_m}, C_{b_m}, and C_{c_m} are the main compensation capacitance of three phases; C_{a_p}, C_{b_p}, and C_{c_p} are the parallel switched capacitance; C_{a_s}, C_{b_s}, and C_{c_s} are the series switched capacitance; M_{a_p}, M_{b_p}, and M_{c_p} are MOSFETs for switching C_{a_p}, C_{b_p}, and C_{c_p}; M_{a_s}, M_{b_s}, and M_{c_s} are MOSFETs for switching C_{a_s}, C_{b_s}, and C_{c_s}; s_{a_p}, s_{b_p}, s_{c_p}, s_{a_s}, s_{b_s}, and s_{c_s} are the PWM driving signal of MOSFETs; C_{o_1} and C_{o_2} are the voltage dividing and stabilizing capacitances.

The design of the control scheme can be divided by function to make the design more efficient. The control scheme corresponding to FIGURE 10 consists of the

capacitive reactance regulation of the switched capacitor, tuning based on the P&O method, and phase difference control of current, which are respectively shown in FIGURE 11 (a), (b), and (c). In the figure, CLK is the clock signal of tuning control, which represents the control speed, $EN1_{a/b/c}$ is the control enable signal of tuning of phase $a/b/c$ based on the P&O method, and $EN2_{a/b/c}$ is the control enable signal of $\theta_{ab/bc/ca}$ for three-phase balance.

The capacitive reactance regulation of the switched capacitor for each phase includes four parts, as shown in FIGURE 11 (a). Part 1) capacitive reactance gain regulation consists of a discrete integrator whose output value $g_{a/b/c}$ represents the capacitive reactance gain. The integrator's output value can increase or decrease the capacitive reactance according to different integration directions provided by the previous stage. The clock signal CLK of the integrator represents the speed of tuning. Part 2) duty cycle calculation is used to calculate the duty cycle of the PWM control signal of the MOSFETs, according to (5) and (9). Here, if $g_{a/b/c} \geq 1$, $g_p = 1$ and $g_s = g_{a/b/c}$. Otherwise, $g_p = g_{a/b/c}$ and $g_s = 1$. Part 3) synchronous sawtooth wave generation is used to generate the sawtooth wave synchronized with the input voltage of the rectifier bridge. Part 4) PWM signal generation is used to generate the control signal of MOSFET according to the synchronous sawtooth wave and duty cycle. Here, due to the non-ideal of the actual devices, the propagation delay of the drive circuit needs to be taken into account to obtain an accurate synchronous control signal, which can be obtained through actual measurement.

The tuning control scheme for each phase based on the P&O method includes three parts, as shown in FIGURE 11 (b). Part 1) U_{out} measurement is used to measure the output voltage, which is the observed object in the P&O control method. Part 2) change observation is used to obtain the changing trend of U_{out}. Part 3) perturbation direction control provides the capacitive reactance regulation direction according to the changing trend of U_{out}.

The control of the current phase difference consists of 1) phase difference measurement and 2) regulation direction control. The first part is used to obtain $\theta_{ab/bc/ca}$ according to the sawtooth wave $Saw_{a/b/c}$ generated in FIGURE 11 (a). The second part controls the capacitive reactance regulation direction according to whether $\theta_{ab/bc/ca}$ is greater than $120°$.

To compare the effects of the above two tuning strategies, the receiver tuning control flow charts for the tuning three phases sequentially and simultaneously are designed and shown in FIGURE 12 (a) and (b), respectively. For the control of tuning three phases sequentially, the tuning of three phases is disabled initially. Then, the three phases are tuned sequentially. For each phase, at the later stage of tuning, $g_{a/b/c}$ changes stably in a fixed range $[g_{a/b/c\_min}, g_{a/b/c\_max}]$. Therefore, it is possible to determine whether tuning is completed by determining whether $g_{a/b/c\_min}$ and $g_{a/b/c\_max}$ are stable. On the other hand, according to the characteristics of the P&O method, the final target of $g_{a/b/c}$ is close to $(g_{a/b/c\_max} + g_{a/b/c\_min})/2$.
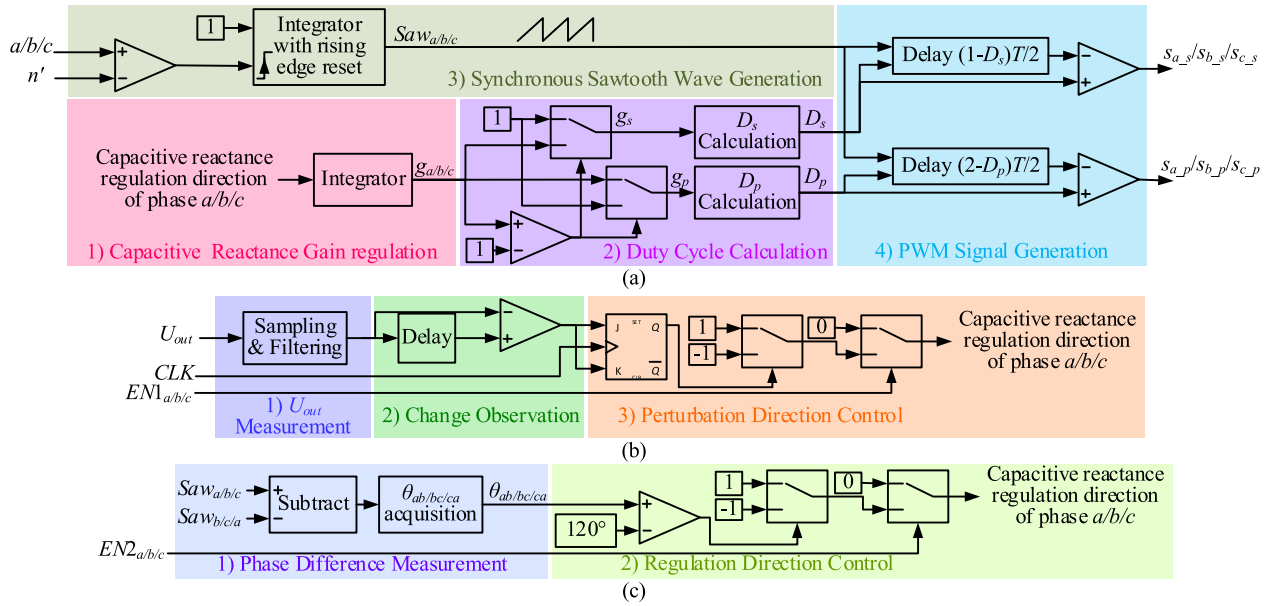
FIGURE 11. Control scheme. (a) the capacitive reactance regulation of switched capacitor, (b) tuning based on the P&O method, and (c) phase difference control of current.
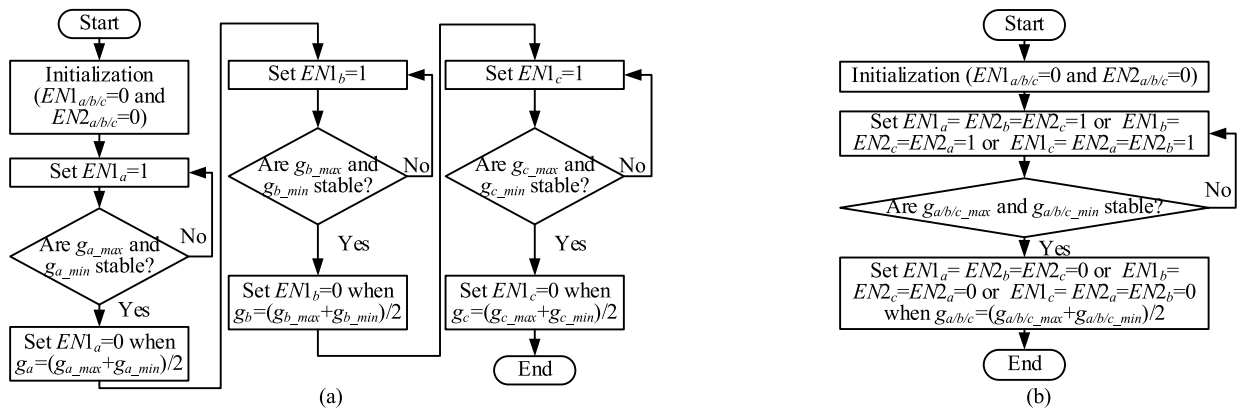

FIGURE 12. Control flow chart of receiver for (a) tuning three phases sequentially and (b) tuning three phases simultaneously.

V. EXPERIMENTAL VERIFICATION

The experimental system built according to the design is shown in FIGURE 13. The switched capacitor was applied in the receiver of a 1:5 scale three-phase meander-type DWPT prototype for rail vehicle applications [9]. The main dimension information of the prototype is shown in the figure. Besides, the number of turns of the receiving coil is 9. The specifications of the Litz wire used in the transmitting coil and the receiving coil are both 0.1mm × 200 strands with an outer diameter of 2.0mm. The air gap between the transmitting coils and receiving coils is 10mm.

The schematic of the three-phase transmitter is shown in FIGURE 14, in which $\dot{I}_A$, $\dot{I}_B$, and $\dot{I}_C$ are the currents of the three-phase transmitting coil, and U_{in} is the DC input voltage. For simplification, LCC (inductor-capacitor-capacitor) compensation topology is applied to maintain the constant current amplitude of the transmitting coils [23], [24]. Nevertheless,

due to the influence of internal resistance and mistuning in the practical system, the current of the transmitting coil will be slightly affected by the load. Therefore, the RMS values of $\dot{I}_A$, $\dot{I}_B$, and $\dot{I}_C$ are maintained at 10.0A by slightly adjusting U_{in} under different output currents in the experiment.

The parameters of the experimental system are listed in TABLE 2 According to the system parameters and (12), the theoretical compensation capacitances for phase a, b, and c receiving coils can be calculated as $C_a' = 69.8nF$, $C_b' = 67.8nF$, $C_c' = 34.3nF$. Generally, capacitors with a manufacturing tolerance of ± 5% (code J) are easy to produce, and higher manufacturing accuracy will lead to a significant cost increase. For example, when the manufacturing tolerance is ±5%, inexpensive film capacitors can be used. Therefore, for verification of tuning, two sets of capacitors with the maximum deviation are purposely configured. One set of capacitances are $C_{a\_m} = 73.8nF$, $C_{b\_m} = 71.2nF$, and
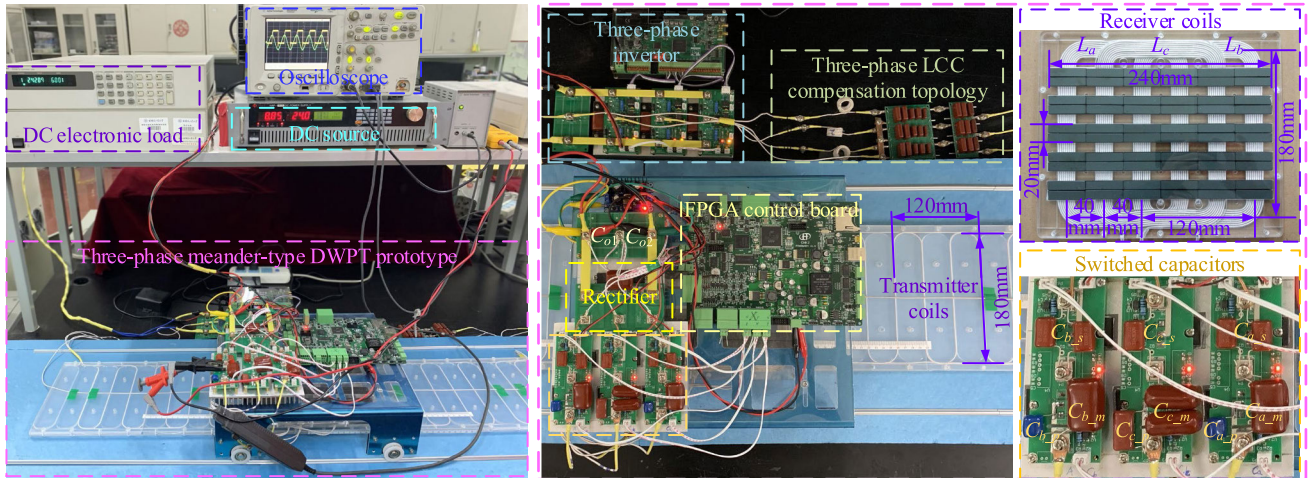
FIGURE 13. Experimental system.

TABLE 2. Parameters Of the experimental system.

| Symbol	Parameter	Value	Unit
f_0	Working frequency	100	kHz
U_{in_0}	Nominal input voltage	24.0	V
U_{out_0}	Ideal design output voltage	27.0	V
C_{i_1}, C_{i_2}	Voltage divider capacitances	10	μF
L_{f_A}, L_{f_B}, L_{f_C}	Compensation inductances	1.50	μH
C_{f_A}, C_{f_B}, C_{f_C}	Parallel compensation capacitances	1.69	μF
C_A, C_B, C_C	Serial compensation capacitances	1.71	μF
L_A, L_B, L_C	Self-inductances of transmitting coils	2.2	μH
L_a	Self-inductance of phase a receiving coil	39.0	μH
L_b	Self-inductance of phase b receiving coil	39.2	μH
L_c	Self-inductance of phase c receiving coil	40.6	μH
r_a	Internal resistance of phase a receiving coil	113	mΩ
r_b	Internal resistance of phase b receiving coil	115	mΩ
r_c	Internal resistance of phase c receiving coil	117	mΩ
M_{ab}	Mutual inductance between phase a and b	2.26	μH
M_{ac}	Mutual inductance between phase a and c	-15.2	μH
M_{bc}	Mutual inductance between phase b and c	-15.7	μH
C_{o_1}, C_{o_2}	Voltage stabilizing capacitance	10	μF
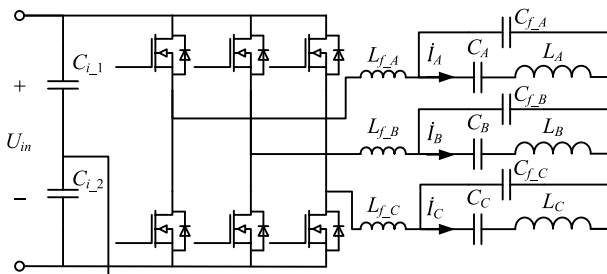
FIGURE 14. Schematic of the three-phase transmitter with LCC compensation topology.

$C_{c\_m} = 36.0$nF, which are 5% larger than the theoretical value, and used to verify the effectiveness of series switched-capacitor tuning. The other set of capacitances are $C_{a\_m} = 66.2$nF, $C_{b\_m} = 64.5$nF, and $C_{c\_m} = 32.8$nF, which are 5% smaller than the theoretical value, and used to verify the effectiveness of parallel switched-capacitor tuning.
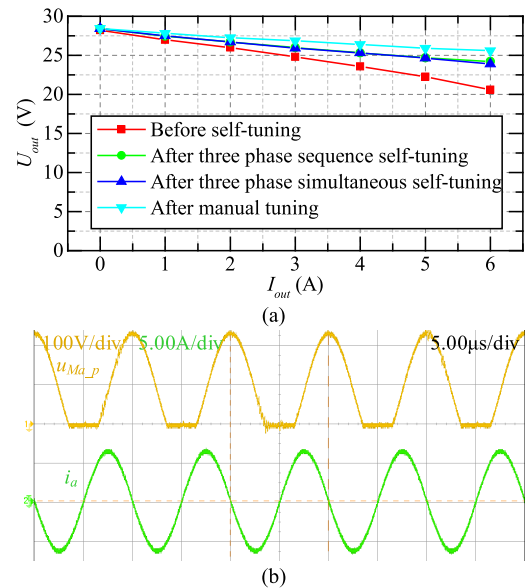
FIGURE 15. When $C_{a\_m} = 66.2$nF, $C_{b\_m} = 64.5$nF, and $C_{c\_m} = 32.8$nF, (a) the output voltage at different output current before and after self-tuning, and (b) the waveform of u_{Ma_p} and i_a at $I_{out} = 6.0$A after tuning.

In a practical system, besides the compensation capacitance, there may be errors in other parts' parameters. To ensure a wide enough calibration range, the parallel switched capacitors are selected according to about one-tenth of the theoretical compensation capacitances, and the series switched capacitors are decided according to about ten times the theoretical compensation capacitances. In this way, the compensation capacitance can be calibrated within the range of about ±10% deviation from the optimal value. On the other side, from the perspective of power flow, the essence of receiver tuning is to avoid reactive power returning to the power supply, which causes reactive power loss at the transmitter. Therefore, to ensure the tuning effect is positive, the equivalent quality factor of the switched capacitor must
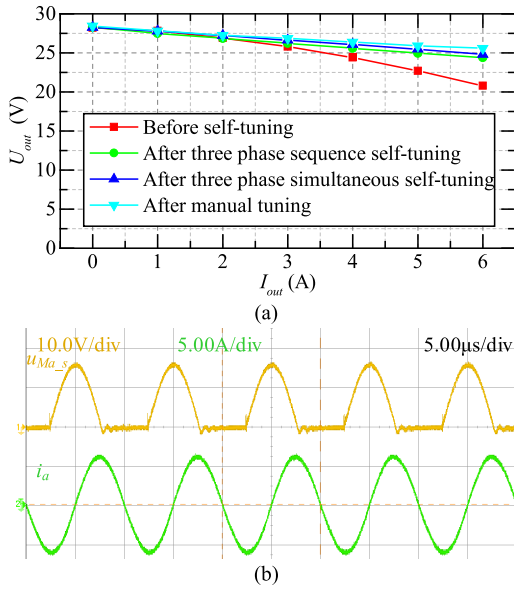
(a)

(b)

FIGURE 16. When C_{a_m} = 73.8nF, C_{b_m} = 71.2nF, and C_{c_m} = 36.0nF, (a) the output voltage at different output current before and after tuning, and (b) the waveform of u_{Ma_s} and i_a at I_{out} = 6.0A after tuning.
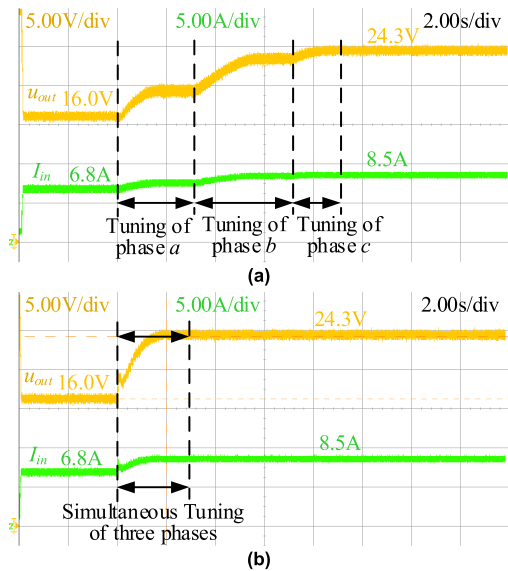

(a)

(b)

FIGURE 17. The waveform of U_{out} and I_{in} in (a) sequential tuning and (b) simultaneous tuning of three phases when C_{a_m} = 73.8nF, C_{b_m} = 71.2nF, C_{c_m} = 36.0nF, U_{in} = 24.0V, and I_{out} = 6.0A.

be greater than the quality factor of the transmitter circuit. Since the quality factors of parallel and series switched capacitors can be approximately calculated as $1/(r_{sw}\omega_0 C_p)$ and $1/(r_{sw}\omega_0 C_s)$ respectively, where r_{sw} is the on-state resistance of switch, to achieve an excellent tuning effect, the on-state resistance of the switches in the parallel and series switched capacitors should be as small as possible. The final configuration of the switched capacitors and the selection of MOSFETs are listed in TABLE 3.

In the experiment, two sets of capacitors were tuned once under different output currents, and the output voltages before

TABLE 3. Configuration of the switched capacitors and selection of mosfets.

Symbol	Parameter	Specifications
C_{a_p}, C_{b_p}	Parallel switched capacitors of phase a, b	682J
C_{c_p}	Parallel switched capacitor of phase c	332J
C_{a_s}, C_{b_s}	Series switched capacitors of phase a, b	Two 334J in parallel
C_{c_s}	Series switched capacitor of phase c	334J
M_{a_p}, M_{b_p}, M_{b_p}	MOSFET for parallel switched capacitor	SPW17N80C3
M_{a_s}, M_{b_s}, M_{b_s}	MOSFET for series switched capacitor	IRFP260N

and after tuning were recorded. The experimental results of the two sets of capacitance are shown in FIGURE 15(a) and FIGURE 16(a), respectively. The output voltage after three-phase sequence self-tuning is almost the same as that of three-phase simultaneous self-tuning. By comparing the experimental results before and after self-tuning, it can be seen that the effect of mistuning can be ignored when the output current is small. Conversely, when the output current is large, the output voltage after tuning is significantly higher than that without tuning. Also, it can be seen that the output voltage after tuning decreases linearly with the output current increase due to the internal resistance of receiving coils, capacitors, MOSFETs, rectifiers, and connectors. The manual tuning experiment is also carried out to compare with the self-tuning. The output voltage at different output currents after manual tuning is also shown in FIGURE 15(a) and FIGURE 16(a). It can be seen that the output voltage after self-tuning decreases quicker than manual tuning with the output current increases. This is because the internal resistance of the circuit is increased due to the switched-capacitors.

Besides, FIGURE 15 (b) and FIGURE 16 (b) show the waveform of u_{Ma_p}, u_{Ma_s}, and i_a at I_{out} = 6.0A after tuning under the condition of small and large compensation capacitance, respectively. Both the waveforms are consistent with FIGURE 2 (b) and FIGURE 4 (b), respectively. The maximum voltage of u_{Ma_p} in FIGURE 15 (b) is significantly higher than that of u_{Ma_p} in FIGURE 16 (b), which indicates that the suitable switching devices for series switched capacitors in high voltage applications can be easily obtained. Note that the waveforms of phase b and c are not given here due to the similarity to phase a.

For the two different control strategies, the waveform of U_{out} and DC input current I_{in} during one round tuning process is shown in FIGURE 17 when C_{a_m} = 73.8nF, C_{b_m} = 71.2nF, C_{c_m} = 36.0nF, U_{in} = 24.0V, and I_{out} = 6.0A. The allover system efficiencies before and after tuning are 59% and 71%, respectively. According to the parameters of devices and the output current, after tuning, the losses of the receiving coil and the switched capacitor can be calculated as 7W and 12W, respectively, and the losses of switches can be ignored. Besides, the measured power consumption of the control board is 4W. Then, the power loss of the transmitter can be calculated as 36W. The main reasons for the low maximum efficiency are the low-quality factor of the used devices at 100kHz and low passive rectification efficiency

at low output voltages. Devices with higher quality factors can be used to improve maximum efficiency. Moreover, for the control method of tuning three phases sequentially, the whole tuning process takes about 9 seconds, while tuning three phases simultaneously only consumes about 3 seconds.

The reason why the tuning time reaches seconds is that the tuning basis of the P&O method is the change of output voltage, and the actual output voltage detection inevitably has interference. A long detection time is needed to measure the output voltage stably and reliably to ensure control accuracy. However, since the self-tuning is designed to be only executed in the static state, the seconds level tuning time is acceptable.

VI. CONCLUSION

To eliminate the mistuning caused by the deviation of the system parameters in the three-phase dynamic wireless power receiver, this paper studies the self-tuning technology of the three-phase wireless power receiver from the perspective of practicability. Based on the idea of tuning when the vehicle is parked on the station, a non-real-time self-tuning scheme is proposed, which is based on the P&O method and switched capacitor. In the proposed self-tuning scheme, the switched capacitor has the advantage of a small volume. On the basis of the parallel switched-capacitor tuning, further analysis shows that the series switched-capacitor tuning is more suitable for high voltage applications and can increase the range of reactance regulation or reduce the device rating when combined with the parallel switched capacitor. In terms of the specific control method, the P&O method is easy to implement due to it does not require the problematic detection of three-phase induced voltage. Moreover, to overcome the shortage of the sequentially tuning of three phases, a faster three-phase simultaneous tuning strategy is proposed by introducing additional current phase difference control. Besides, the required additional current phase detection circuit for simultaneous tuning is multiplexed with that of the switched capacitor, which avoids the increase in system structure complexity and cost. The experimental results show that the mistuning effect on the output voltage can be neglected after self-tuning, and the speed of the proposed simultaneous tuning strategy of three phases is about three times that of the conventional strategy. According to the analysis and experimental results, the switched capacitor self-tuning scheme for three-phase systems based on the P&O method has a good tuning effect and practicability.

REFERENCES

[1] G. A. Covic and J. T. Boys, "Inductive power transfer," *Proc. IEEE*, vol. 101, no. 6, pp. 1276–1289, Jun. 2013.

[2] C. C. Mi, G. Buja, S. Y. Choi, and C. T. Rim, "Modern advances in wireless power transfer systems for roadway powered electric vehicles," *IEEE Trans. Ind. Electron.*, vol. 63, no. 10, pp. 6533–6545, Oct. 2016.

[3] A. Ahmad, M. S. Alam, and R. Chabaan, "A comprehensive review of wireless charging technologies for electric vehicles," *IEEE Trans. Transport. Electrific.*, vol. 4, no. 1, pp. 38–63, Mar. 2018.

[4] D. Patil, M. K. McDonough, J. M. Miller, B. Fahimi, and P. T. Balsara, "Wireless power transfer for vehicular applications: Overview and challenges," *IEEE Trans. Transport. Electrific.*, vol. 4, no. 1, pp. 3–37, Mar. 2018.

[5] X. Dai, J.-C. Jiang, and J.-Q. Wu, "Charging area determining and power enhancement method for multiexcitation unit configuration of wirelessly dynamic charging EV system," *IEEE Trans. Ind. Electron.*, vol. 66, no. 5, pp. 4086–4096, May 2019.

[6] A. Zaheer, M. Neath, H. Z. Z. Beh, and G. A. Covic, "A dynamic EV charging system for slow moving traffic applications," *IEEE Trans. Transport. Electrific.*, vol. 3, no. 2, pp. 354–369, Jun. 2017.

[7] A. Kamineni, M. J. Neath, G. A. Covic, and J. T. Boys, "A mistuning-tolerant and controllable power supply for roadway wireless power systems," *IEEE Trans. Power Electron.*, vol. 32, no. 9, pp. 6689–6699, Sep. 2017.

[8] U. Iruretagoyena, I. Villar, A. Garcia-Bediaga, L. Mir, and H. Camblong, "Design and characterization of a meander-type dynamic inductively coupled power transfer coil," *IEEE Trans. Ind. Appl.*, vol. 53, no. 4, pp. 3950–3959, Jul. 2017.

[9] C. Wang, C. Zhu, G. Wei, J. Feng, J. Jiang, and R. Lu, "Design of compact three-phase receiver for meander-type dynamic wireless power transfer system," *IEEE Trans. Power Electron.*, vol. 35, no. 7, pp. 6854–6866, Jul. 2020.

[10] S. Cui, Z. Wang, S. Han, C. Zhu, and C. C. Chan, "Analysis and design of multiphase receiver with reduction of output fluctuation for EV dynamic wireless charging system," *IEEE Trans. Power Electron.*, vol. 34, no. 5, pp. 4112–4124, May 2019.

[11] R. Mai, P. Yue, Y. Liu, Y. Zhang, and Z. He, "A dynamic tuning method utilizing inductor paralleled with load for inductive power transfer," *IEEE Trans. Power Electron.*, vol. 33, no. 12, pp. 10924–10934, Dec. 2018.

[12] D.-H. Kim and D. Ahn, "Self-tuning LCC inverter using PWM-controlled switched capacitor for inductive wireless power transfer," *IEEE Trans. Ind. Electron.*, vol. 66, no. 5, pp. 3983–3992, May 2019.

[13] J.-U.-W. Hsu, A. P. Hu, and A. Swain, "A wireless power pickup based on directional tuning control of magnetic amplifier," *IEEE Trans. Ind. Electron.*, vol. 56, no. 7, pp. 2771–2781, Jul. 2009.

[14] K. A. Cota, P. A. Gray, M. Pathmanathan, and P. W. Lehn, "An approach for selecting compensation capacitances in resonance-based EV wireless power transfer systems with switched capacitors," *IEEE Trans. Transport. Electrific.*, vol. 5, no. 4, pp. 1004–1014, Dec. 2019.

[15] A. Kamineni, G. A. Covic, and J. T. Boys, "Self-tuning power supply for inductive charging," *IEEE Trans. Power Electron.*, vol. 32, no. 5, pp. 3467–3479, May 2017.

[16] T. C. Beh, M. Kato, T. Imura, S. Oh, and Y. Hori, "Automated impedance matching system for robust wireless power transfer via magnetic resonance coupling," *IEEE Trans. Ind. Electron.*, vol. 60, no. 9, pp. 3689–3698, Sep. 2013.

[17] R. W. Porto, V. J. Brusamarello, L. A. Pereira, and F. R. de Sousa, "Fine tuning of an inductive link through a voltage-controlled capacitance," *IEEE Trans. Power Electron.*, vol. 32, no. 5, pp. 4115–4124, May 2017.

[18] H. Kennedy, R. Bodnar, T. Lee, and W. Redman-White, "A self-tuning resonant-inductive-link transmit driver using quadrature symmetric delay trimmable phase-switched fractional capacitance," *IEEE J. Solid-State Circuits*, vol. 53, no. 6, pp. 1694–1706, Jun. 2018.

[19] R. Mai, Y. Liu, Y. Li, P. Yue, G. Cao, and Z. He, "An active-rectifier-based maximum efficiency tracking method using an additional measurement coil for wireless power transfer," *IEEE Trans. Power Electron.*, vol. 33, no. 1, pp. 716–728, Jan. 2018.

[20] Z. Li, S. Dong, K. Song, C. Zhu, Q. Zhang, and X. Huang, "Adaptive position alignment for wireless charging system with mutual inductance estimation and P&O algorithms employ only primary-side electrical parameters," *IET Power Electron.*, vol. 12, no. 10, pp. 2493–2500, Aug. 2019.

[21] R. Arnold and P. Gratzfeld, "Automatic tuning concept for a three-phase inductive power transfer system," in *Proc. 4th Int. Electr. Drives Prod. Conf. (EDPC)*, Nuremberg, Germany, Sep. 2014, pp. 1–7.

[22] A. Safaee, K. Woronowicz, and T. Dickson, "Reactive power compensation in three phase high output inductive power transfer," in *Proc. IEEE Electr. Power Energy Conf. (EPEC)*, London, ON, Canada, Oct. 2015, pp. 375–380.

[23] Q. Zhu, L. Wang, Y. Guo, C. Liao, and F. Li, "Applying LCC compensation network to dynamic wireless EV charging system," *IEEE Trans. Ind. Electron.*, vol. 63, no. 10, pp. 6557–6567, Oct. 2016.

[24] S. Zhou, C. Zhu, S. Cui, Z. Wang, S. Zhou, and C. C. Chan, "Dynamic wireless power transfer system for electric vehicles employing multiplexing LCC modules with individual transmitters," *IEEE Access*, vol. 6, pp. 62514–62527, Oct. 2018.

[25] Z. Huang, C.-S. Lam, P.-I. Mak, R. P. D. S. Martins, S.-C. Wong, and C. K. Tse, "A single-stage inductive-power-transfer converter for constant-power and maximum-efficiency battery charging," *IEEE Trans. Power Electron.*, vol. 35, no. 9, pp. 8973–8984, Sep. 2020.

CHAO WANG received the B.S. degree in measurement and control technology and instrument from Nanchang University, Nanchang, China, in 2014. He is currently pursuing the Ph.D. degree in electrical engineering with the Harbin Institute of Technology, Harbin, China.

His research interests include wireless power transfer and dynamic wireless charging for electric vehicles.

JINGYANG ZHANG received the B.S. degree in measurement and control technology and instrument, and the M.E. degree in instruments science and technology from the Harbin Institute of Technology, Harbin, China, in 2017 and 2019, respectively. His research interest includes wireless power transfer.

CHUNBO ZHU (Member, IEEE) received the B.S. and M.S. degrees in electrical engineering and the Ph.D. degree in mechanical engineering from the Harbin Institute of Technology (HIT), Harbin, China, in 1987, 1992, and 2001, respectively.

From 2003 to 2004, he was a Postdoctoral Research Fellow with the PEI Research Center, National University of Ireland, Galway, Ireland. Since 1987, he has been a Lecturer with the Department of Automation Measurement and Control, HIT. He is currently a Full Professor with HIT, where he leads the Laboratory of Wireless Power Transfer and Battery Management Technologies. His current research interests include energy management systems, electric and hybrid electric vehicles, and wireless power transfer technologies.

GUO WEI received the M.S. degree in electrical engineering from the Harbin Institute of Technology, Harbin, China, in 1991, and the Ph.D. degree in electrical engineering from Saga University, Honjomachi, Japan, in 2003.

He is currently a Professor with the Harbin Institute of Technology. His main research interests include wireless power and information transfer, sensing technology, instrumentation, and signal processing.

FEI LIU was born in Hebei, China, in 1981. He received the master's degree in power electronics and electric drive from Beijing Jiaotong University, in 2008. He is currently working at China Academy of Launch Vehicle Technology, Beijing, China, and is mainly engaged in the aircraft avionics system and power system design and optimization.

• • •